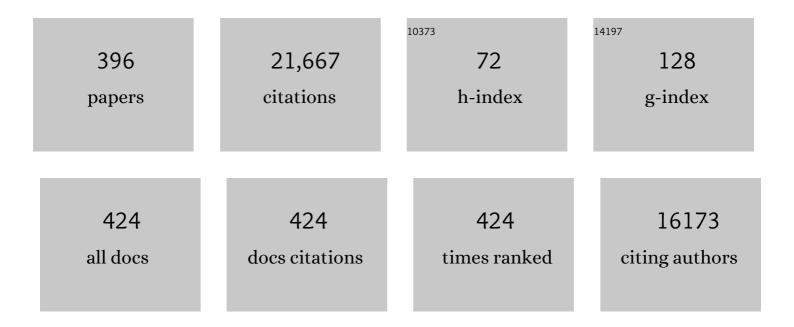
## **Richard E Carson**

List of Publications by Year in descending order

Source: https://exaly.com/author-pdf/6863997/publications.pdf Version: 2024-02-01



#	Article	IF	CITATIONS
1	Consensus Nomenclature for in vivo Imaging of Reversibly Binding Radioligands. Journal of Cerebral Blood Flow and Metabolism, 2007, 27, 1533-1539.	2.4	1,840
2	Reduced prefrontal activity predicts exaggerated striatal dopaminergic function in schizophrenia. Nature Neuroscience, 2002, 5, 267-271.	7.1	603
3	Dissociated Pattern of Activity in Visual Cortices and Their Projections During Human Rapid Eye Movement Sleep. Science, 1998, 279, 91-95.	6.0	584
4	Linearized Reference Tissue Parametric Imaging Methods: Application to [11C]DASB Positron Emission Tomography Studies of the Serotonin Transporter in Human Brain. Journal of Cerebral Blood Flow and Metabolism, 2003, 23, 1096-1112.	2.4	574
5	Noise Reduction in the Simplified Reference Tissue Model for Neuroreceptor Functional Imaging. Journal of Cerebral Blood Flow and Metabolism, 2002, 22, 1440-1452.	2.4	353
6	Reduced Serotonin Type 1A Receptor Binding in Panic Disorder. Journal of Neuroscience, 2004, 24, 589-591.	1.7	350
7	Comparison of Bolus and Infusion Methods for Receptor Quantitation: Application to [ <sup>18</sup> F]Cyclofoxy and Positron Emission Tomography. Journal of Cerebral Blood Flow and Metabolism, 1993, 13, 24-42.	2.4	343
8	Imaging synaptic density in the living human brain. Science Translational Medicine, 2016, 8, 348ra96.	5.8	343
9	Caloric restriction increases neurotrophic factor levels and attenuates neurochemical and behavioral deficits in a primate model of Parkinson's disease. Proceedings of the National Academy of Sciences of the United States of America, 2004, 101, 18171-18176.	3.3	334
10	Species-specific calls evoke asymmetric activity in the monkey's temporal poles. Nature, 2004, 427, 448-451.	13.7	324
11	Deficits in Prefrontal Cortical and Extrastriatal Dopamine Release in Schizophrenia. JAMA Psychiatry, 2015, 72, 316.	6.0	304
12	Assessing Synaptic Density in Alzheimer Disease With Synaptic Vesicle Glycoprotein 2A Positron Emission Tomographic Imaging. JAMA Neurology, 2018, 75, 1215.	4.5	304
13	Strategies to Improve Neuroreceptor Parameter Estimation by Linear Regression Analysis. Journal of Cerebral Blood Flow and Metabolism, 2002, 22, 1271-1281.	2.4	286
14	Lower synaptic density is associated with depression severity and network alterations. Nature Communications, 2019, 10, 1529.	5.8	277
15	Imaging robust microglial activation after lipopolysaccharide administration in humans with PET. Proceedings of the National Academy of Sciences of the United States of America, 2015, 112, 12468-12473.	3.3	265
16	Long-Term Clinical Improvement in MPTP-Lesioned Primates after Gene Therapy with AAV-hAADC. Molecular Therapy, 2006, 14, 564-570.	3.7	249
17	Quantification of Amphetamine-Induced Changes in [11C]Raclopride Binding with Continuous Infusion. Journal of Cerebral Blood Flow and Metabolism, 1997, 17, 437-447.	2.4	237
18	Highly penetrative, drug-loaded nanocarriers improve treatment of glioblastoma. Proceedings of the National Academy of Sciences of the United States of America, 2013, 110, 11751-11756.	3.3	222

#	Article	IF	CITATIONS
19	Clinically Relevant Doses of Methylphenidate Significantly Occupy Norepinephrine Transporters in Humans In Vivo. Biological Psychiatry, 2010, 68, 854-860.	0.7	201
20	Synthesis and Preclinical Evaluation of <sup>11</sup> C-UCB-J as a PET Tracer for Imaging the Synaptic Vesicle Clycoprotein 2A in the Brain. Journal of Nuclear Medicine, 2016, 57, 777-784.	2.8	197
21	Kinetic Modeling of [11C]Raclopride: Combined PET-Microdialysis Studies. Journal of Cerebral Blood Flow and Metabolism, 1997, 17, 932-942.	2.4	183
22	The neuroinflammation marker translocator protein is not elevated in individuals with mild-to-moderate depression: A [11C]PBR28 PET study. Brain, Behavior, and Immunity, 2013, 33, 131-138.	2.0	180
23	Endotoxin-induced systemic inflammation activates microglia: [11C]PBR28 positron emission tomography in nonhuman primates. NeuroImage, 2012, 63, 232-239.	2.1	179
24	A Noninvasive Positron Computed Tomography Technique Using Oxygen-15-Labeled Water for the Evaluation of Neurobehavioral Task Batteries. Journal of Cerebral Blood Flow and Metabolism, 1985, 5, 70-78.	2.4	171
25	In vivo measurement of widespread synaptic loss in Alzheimer's disease with SV2A PET. Alzheimer's and Dementia, 2020, 16, 974-982.	0.4	170
26	The Functional Neuroanatomy of Tourette's Syndrome: An FDG-PET Study. I. Regional Changes in Cerebral Glucose Metabolism Differentiating Patients and Controls. Neuropsychopharmacology, 1993, 9, 277-291.	2.8	166
27	Widespread abnormality of the Î <sup>3</sup> -aminobutyric acid-ergic system in Tourette syndrome. Brain, 2012, 135, 1926-1936.	3.7	166
28	Imaging Neuroinflammation in Alzheimer's Disease with Radiolabeled Arachidonic Acid and PET. Journal of Nuclear Medicine, 2008, 49, 1414-1421.	2.8	158
29	Imaging incorporation of circulating docosahexaenoic acid into the human brain using positron emission tomography. Journal of Lipid Research, 2009, 50, 1259-1268.	2.0	156
30	Kinetic evaluation and test–retest reproducibility of [ <sup>11</sup> C]UCB-J, a novel radioligand for positron emission tomography imaging of synaptic vesicle glycoprotein 2A in humans. Journal of Cerebral Blood Flow and Metabolism, 2018, 38, 2041-2052.	2.4	143
31	Dissociation of Object and Spatial Vision in Human Extrastriate Cortex: Age-Related Changes in Activation of Regional Cerebral Blood Flow Measured with [15 O]Water and Positron Emission Tomography. Journal of Cognitive Neuroscience, 1992, 4, 23-34.	1.1	140
32	Rapid Changes in Cannabinoid 1 Receptor Availability in Cannabis-Dependent Male Subjects After Abstinence From Cannabis. Biological Psychiatry: Cognitive Neuroscience and Neuroimaging, 2016, 1, 60-67.	1.1	135
33	Brivaracetam, a selective highâ€affinity synaptic vesicle protein 2A ( <scp>SV</scp> 2A) ligand with preclinical evidence of high brain permeability and fast onset of action. Epilepsia, 2016, 57, 201-209.	2.6	130
34	Examination of Blood — Brain Barrier Permeability in Dementia of the Alzheimer Type with [ <sup>68</sup> Ga]EDTA and Positron Emission Tomography. Journal of Cerebral Blood Flow and Metabolism, 1987, 7, 1-8.	2.4	129
35	Tomographic mapping of human cerebral metabolism: Sensory deprivation. Annals of Neurology, 1982, 12, 435-444.	2.8	127
36	Measurement of Local Blood Flow and Distribution Volume with Short-Lived Isotopes: A General Input Technique. Journal of Cerebral Blood Flow and Metabolism, 1982, 2, 99-108.	2.4	123

#	Article	IF	CITATIONS
37	Toward an evolutionary perspective on conceptual representation: Species-specific calls activate visual and affective processing systems in the macaque. Proceedings of the National Academy of Sciences of the United States of America, 2004, 101, 17516-17521.	3.3	118
38	Association of Posttraumatic Stress Disorder With Reduced In Vivo Norepinephrine Transporter Availability in the Locus Coeruleus. JAMA Psychiatry, 2013, 70, 1199.	6.0	116
39	Development of Fluorine-18-Labeled 5-HT1AAntagonists. Journal of Medicinal Chemistry, 1999, 42, 1576-1586.	2.9	112
40	PET imaging of the effects of age and cocaine on the norepinephrine transporter in the human brain using (S,S)-[ <sup>11</sup> C]O-methylreboxetine and HRRT. Synapse, 2010, 64, 30-38.	0.6	112
41	Synaptic Changes in Parkinson Disease Assessed with in vivo Imaging. Annals of Neurology, 2020, 87, 329-338.	2.8	112
42	Noise Reduction in the Simplified Reference Tissue Model for Neuroreceptor Functional Imaging. Journal of Cerebral Blood Flow and Metabolism, 2002, , 1440-1452.	2.4	110
43	In Vivo Imaging of Endogenous Pancreatic β-Cell Mass in Healthy and Type 1 Diabetic Subjects Using <sup>18</sup> F-Fluoropropyl-Dihydrotetrabenazine and PET. Journal of Nuclear Medicine, 2012, 53, 908-916.	2.8	108
44	Altered metabotropic glutamate receptor 5 markers in PTSD: In vivo and postmortem evidence. Proceedings of the National Academy of Sciences of the United States of America, 2017, 114, 8390-8395.	3.3	107
45	Weighted Integration Method for Local Cerebral Blood Flow Measurements with Positron Emission Tomography. Journal of Cerebral Blood Flow and Metabolism, 1986, 6, 245-258.	2.4	106
46	Reduced Muscarinic Type 2 Receptor Binding in Subjects With Bipolar Disorder. Archives of General Psychiatry, 2006, 63, 741.	13.8	106
47	Activation of cerebral blood flow during a visuoperceptual task in patients with Alzheimer-type dementia. Neurobiology of Aging, 1993, 14, 35-44.	1.5	103
48	Altered Cerebral γ-Aminobutyric Acid Type A–Benzodiazepine Receptor Binding in Panic Disorder Determined by [11C]Flumazenil Positron Emission Tomography. Archives of General Psychiatry, 2008, 65, 1166.	13.8	103
49	Increased Nanoparticle Delivery to Brain Tumors by Autocatalytic Priming for Improved Treatment and Imaging. ACS Nano, 2016, 10, 4209-4218.	7.3	103
50	Preferential binding to dopamine D3 over D2 receptors by cariprazine in patients with schizophrenia using PET with the D3/D2 receptor ligand [11C]-(+)-PHNO. Psychopharmacology, 2016, 233, 3503-3512.	1.5	101
51	Glucose Metabolism in the Insula and Cingulate Is Affected by Systemic Inflammation in Humans. Journal of Nuclear Medicine, 2012, 53, 601-607.	2.8	100
52	Quantification and pharmacokinetics of blood-brain barrier disruption in humans. Journal of Neurosurgery, 1996, 85, 1056-1065.	0.9	98
53	Muscarinic Cholinergic Receptor Measurements with [18F]FP-TZTP: Control and Competition Studies. Journal of Cerebral Blood Flow and Metabolism, 1998, 18, 1130-1142.	2.4	98
54	A Maximum Likelihood Method for Region-of-Interest Evaluation in Emission Tomography. Journal of Computer Assisted Tomography, 1986, 10, 654-663.	0.5	96

#	Article	IF	CITATIONS
55	5-HT 1A receptors are reduced in temporal lobe epilepsy after partial-volume correction. Journal of Nuclear Medicine, 2005, 46, 1128-35.	2.8	92
56	Tracer Kinetic Modeling in PET. , 2005, , 127-159.		91
57	Biodistribution and Radiation Dosimetry of LMI1195: First-in-Human Study of a Novel <sup>18</sup> F-Labeled Tracer for Imaging Myocardial Innervation. Journal of Nuclear Medicine, 2014, 55, 1445-1451.	2.8	91
58	Recovery from chronic spinal cord contusion after nogo receptor intervention. Annals of Neurology, 2011, 70, 805-821.	2.8	87
59	The Effect of Early Trauma Exposure on Serotonin Type 1B Receptor Expression Revealed by Reduced Selective Radioligand Binding. Archives of General Psychiatry, 2011, 68, 892.	13.8	84
60	Strategies to Improve Neuroreceptor Parameter Estimation by Linear Regression Analysis. Journal of Cerebral Blood Flow and Metabolism, 2002, , 1271-1281.	2.4	84
61	Pet physiological measurements using constant infusion. Nuclear Medicine and Biology, 2000, 27, 657-660.	0.3	83
62	Kinetic Modeling of the Serotonin 5-HT <sub>1B</sub> Receptor Radioligand [ <sup>11</sup> C]P943 in Humans. Journal of Cerebral Blood Flow and Metabolism, 2010, 30, 196-210.	2.4	83
63	Evaluation of motion correction methods in human brain PET imaging—A simulation study based on human motion data. Medical Physics, 2013, 40, 102503.	1.6	83
64	Reduced Brain Cannabinoid Receptor Availability in Schizophrenia. Biological Psychiatry, 2016, 79, 997-1005.	0.7	83
65	Lateralization and gender differences in the dopaminergic response to unpredictable reward in the human ventral striatum. European Journal of Neuroscience, 2011, 33, 1706-1715.	1.2	82
66	In Vivo Ketamine-Induced Changes in [ 11 C]ABP688 Binding to Metabotropic Glutamate Receptor Subtype 5. Biological Psychiatry, 2015, 77, 266-275.	0.7	82
67	All Analysis of Signal Amplification Using Small Detectors in Positron Emission Tomography. Journal of Computer Assisted Tomography, 1982, 6, 551-565.	0.5	80
68	Synthesis and Evaluation of 11C-LY2795050 as a κ-Opioid Receptor Antagonist Radiotracer for PET Imaging. Journal of Nuclear Medicine, 2013, 54, 455-463.	2.8	80
69	Comment: The EM Parametric Image Reconstruction Algorithm. Journal of the American Statistical Association, 1985, 80, 20-22.	1.8	79
70	Reduced Amygdala Serotonin Transporter Binding in Posttraumatic Stress Disorder. Biological Psychiatry, 2011, 70, 1033-1038.	0.7	79
71	Imaging the Cannabinoid CB1 Receptor in Humans with [ <sup>11</sup> C] OMAR: Assessment of Kinetic Analysis Methods, Test–Retest Reproducibility, and Gender Differences. Journal of Cerebral Blood Flow and Metabolism, 2015, 35, 1313-1322.	2.4	79
72	Kinetic Analysis of the 5-HT2A Ligand [11C]MDL 100,907. Journal of Cerebral Blood Flow and Metabolism, 2000, 20, 899-909.	2.4	78

#	Article	IF	CITATIONS
73	11C-PBR28 imaging in multiple sclerosis patients and healthy controls: test-retest reproducibility and focal visualization of active white matter areas. European Journal of Nuclear Medicine and Molecular Imaging, 2015, 42, 1081-1092.	3.3	77
74	Assessment of a white matter reference region for <sup>11</sup> C-UCB-J PET quantification. Journal of Cerebral Blood Flow and Metabolism, 2020, 40, 1890-1901.	2.4	77
75	Brain incorporation of 11C-arachidonic acid, blood volume, and blood flow in healthy aging: a study with partial-volume correction. Journal of Nuclear Medicine, 2004, 45, 1471-9.	2.8	76
76	Cerebral Glucose Metabolism as a Function of Age in Man: Influence of the Rate Constants in the Fluorodeoxyglucose Method. Journal of Cerebral Blood Flow and Metabolism, 1983, 3, 250-253.	2.4	75
77	Reproducibility of Resting Cerebral Blood Flow Measurements with H <sub>2</sub> <sup>15</sup> O Positron Emission Tomography in Humans. Journal of Cerebral Blood Flow and Metabolism, 1993, 13, 748-754.	2.4	75
78	The Functional Neuroanatomy of Tourette's Syndrome: An FDG-PET Study. II: Relationships between Regional Cerebral Metabolism and Associated Behavioral and Cognitive Features of the Illness. Neuropsychopharmacology, 1995, 13, 151-168.	2.8	75
79	The Suitability of [11C]-α-Methyl-L-tryptophan as a Tracer for Serotonin Synthesis: Studies With Dual Administration of [11C] and [14C] Labeled Tracer. Journal of Cerebral Blood Flow and Metabolism, 2000, 20, 244-252.	2.4	74
80	Affinity and selectivity of [ <sup>11</sup> C]â€(+)â€₽HNO for the D3 and D2 receptors in the rhesus monkey brain in vivo. Synapse, 2012, 66, 489-500.	0.6	74
81	Assessment of Dynamic Neurotransmitter Changes with Bolus or Infusion Delivery of Neuroreceptor Ligands. Journal of Cerebral Blood Flow and Metabolism, 1998, 18, 1196-1210.	2.4	72
82	PET evaluation of [18F]FCWAY, an analog of the 5-HT1A receptor antagonist, WAY-100635. Nuclear Medicine and Biology, 2000, 27, 493-497.	0.3	71
83	Effects of Early-Life Stress on Serotonin1A Receptors in Juvenile Rhesus Monkeys Measured by Positron Emission Tomography. Biological Psychiatry, 2010, 67, 1146-1153.	0.7	71
84	No Change in Serotonin Type 1A Receptor Binding in Patients With Posttraumatic Stress Disorder. American Journal of Psychiatry, 2005, 162, 383-385.	4.0	70
85	Effects of age, BMI and sex on the glial cell marker TSPO — a multicentre [11C]PBR28 HRRT PET study. European Journal of Nuclear Medicine and Molecular Imaging, 2019, 46, 2329-2338.	3.3	70
86	Synthesis and <i>in Vivo</i> Evaluation of a Novel PET Radiotracer for Imaging of Synaptic Vesicle Glycoprotein 2A (SV2A) in Nonhuman Primates. ACS Chemical Neuroscience, 2019, 10, 1544-1554.	1.7	70
87	Serotonin 1B Receptor Imaging in Alcohol Dependence. Biological Psychiatry, 2010, 67, 800-803.	0.7	69
88	PET imaging of opiate receptor binding in human epilepsy using [18F]cyclofoxy. Epilepsy Research, 1992, 13, 129-139.	0.8	68
89	Association of In Vivo κ-Opioid Receptor Availability and the Transdiagnostic Dimensional Expression of Trauma-Related Psychopathology. JAMA Psychiatry, 2014, 71, 1262.	6.0	67
90	Imaging Glutamate Homeostasis in Cocaine Addiction with the Metabotropic Glutamate Receptor 5 Positron Emission Tomography Radiotracer [11C]ABP688 and Magnetic Resonance Spectroscopy. Biological Psychiatry, 2014, 75, 165-171.	0.7	66

#	Article	IF	CITATIONS
91	In vivo muscarinic 2 receptor imaging in cognitively normal young and older volunteers. Synapse, 2003, 48, 39-44.	0.6	64
92	Brain Incorporation of [ <sup>11</sup> C]Arachidonic Acid in Young Healthy Humans Measured with Positron Emission Tomography. Journal of Cerebral Blood Flow and Metabolism, 2002, 22, 1453-1462.	2.4	63
93	Dopamine D3 receptor alterations in cocaine-dependent humans imaged with [11C](+)PHNO. Drug and Alcohol Dependence, 2014, 139, 100-105.	1.6	63
94	Kinetic Analysis of the Metabotropic Glutamate Subtype 5 Tracer [ <sup>18</sup> F]FPEB in Bolus and Bolus-Plus-Constant-Infusion Studies in Humans. Journal of Cerebral Blood Flow and Metabolism, 2013, 33, 532-541.	2.4	61
95	First-in-Human Evaluation of <sup>18</sup> F-SynVesT-1, a Radioligand for PET Imaging of Synaptic Vesicle Glycoprotein 2A. Journal of Nuclear Medicine, 2021, 62, 561-567.	2.8	60
96	Intravascular streaming during carotid artery infusions. Journal of Neurosurgery, 1991, 74, 763-772.	0.9	59
97	Higher in vivo muscarinic-2 receptor distribution volumes in aging subjects with an apolipoprotein E-?4 allele. Synapse, 2003, 49, 150-156.	0.6	59
98	Arterial transit time effects in pulsed arterial spin labeling CBF mapping: Insight from a PET and MR study in normal human subjects. Magnetic Resonance in Medicine, 2010, 63, 374-384.	1.9	58
99	Nicotine-Induced Dopamine Release in Primates Measured with [11C]Raclopride PET. Neuropsychopharmacology, 2004, 29, 259-268.	2.8	57
100	The Effect of Antiepileptic Drugs on 5-HT1A-Receptor Binding Measured by Positron Emission Tomography. Epilepsia, 2006, 47, 499-503.	2.6	57
101	In Vivo Synaptic Density Imaging with <sup>11</sup> C-UCB-J Detects Treatment Effects of Saracatinib in a Mouse Model of Alzheimer Disease. Journal of Nuclear Medicine, 2019, 60, 1780-1786.	2.8	57
102	PTSD is associated with neuroimmune suppression: evidence from PET imaging and postmortem transcriptomic studies. Nature Communications, 2020, 11, 2360.	5.8	56
103	List-Mode PET Motion Correction Using Markerless Head Tracking: Proof-of-Concept With Scans of Human Subject. IEEE Transactions on Medical Imaging, 2013, 32, 200-209.	5.4	55
104	Synaptic density and cognitive performance in Alzheimer's disease: A PET imaging study with [ <sup>11</sup> C]UCBâ€J. Alzheimer's and Dementia, 2022, 18, 2527-2536.	0.4	55
105	Pancreatic Beta Cell Mass PET Imaging and Quantification with [11C]DTBZ and [18F]FP-(+)-DTBZ in Rodent Models of Diabetes. Molecular Imaging and Biology, 2011, 13, 973-984.	1.3	54
106	Evaluation of the agonist PET radioligand [11C]GR103545 to image kappa opioid receptor in humans: Kinetic model selection, test–retest reproducibility and receptor occupancy by the antagonist PF-04455242. NeuroImage, 2014, 99, 69-79.	2.1	54
107	Respiratory Motion Compensation for PET/CT with Motion Information Derived from Matched Attenuation-Corrected Gated PET Data. Journal of Nuclear Medicine, 2018, 59, 1480-1486.	2.8	54
108	Anti-edema and antioxidant combination therapy for ischemic stroke via glyburide-loaded betulinic acid nanoparticles. Theranostics, 2019, 9, 6991-7002.	4.6	54

7

#	Article	IF	CITATIONS
109	Positron Emission Tomography Shows Elevated Cannabinoid <scp>CB</scp> <sub>1</sub> Receptor Binding in Men with Alcohol Dependence. Alcoholism: Clinical and Experimental Research, 2012, 36, 2104-2109.	1.4	53
110	Association of Al̂² deposition and regional synaptic density in early Alzheimer's disease: a PET imaging study with [11C]UCB-J. Alzheimer's Research and Therapy, 2021, 13, 11.	3.0	53
111	Cerebral blood flow with [ <sup>15</sup> 0]water PET studies using an image-derived input function and MR-defined carotid centerlines. Physics in Medicine and Biology, 2013, 58, 1903-1923.	1.6	51
112	Reduced synaptic vesicle protein 2A binding in temporal lobe epilepsy: A [ <sup>11</sup> C]UCBâ€J positron emission tomography study. Epilepsia, 2020, 61, 2183-2193.	2.6	51
113	In vivo evidence of lower synaptic vesicle density in schizophrenia. Molecular Psychiatry, 2021, 26, 7690-7698.	4.1	51
114	Evaluation of [11C]MRB for assessment of occupancy of norepinephrine transporters: Studies with atomoxetine in non-human primates. NeuroImage, 2011, 56, 268-279.	2.1	50
115	Phosphodiesterase 10A PET Radioligand Development Program: From Pig to Human. Journal of Nuclear Medicine, 2014, 55, 595-601.	2.8	50
116	Reductions in Brain 5-HT1B Receptor Availability in Primarily Cocaine-Dependent Humans. Biological Psychiatry, 2014, 76, 816-822.	0.7	50
117	Distribution and Kinetics of 3-O-Methyl-6-[18F]fluoro-L-DOPA in the Rhesus Monkey Brain. Journal of Cerebral Blood Flow and Metabolism, 1991, 11, 726-734.	2.4	49
118	InÂvivo variation in same-day estimates of metabotropic glutamate receptor subtype 5 binding using [ <sup>11</sup> C]ABP688 and [ <sup>18</sup> F]FPEB. Journal of Cerebral Blood Flow and Metabolism, 2017, 37, 2716-2727.	2.4	49
119	Human Positron Emission Tomography Neuroimaging. Annual Review of Biomedical Engineering, 2019, 21, 551-581.	5.7	48
120	Opiate receptor avidity and cerebral blood flow in Alzheimer's disease. Journal of the Neurological Sciences, 1997, 148, 171-180.	0.3	47
121	List-mode reconstruction for the Biograph mCT with physics modeling and event-by-event motion correction. Physics in Medicine and Biology, 2013, 58, 5567-5591.	1.6	47
122	Elevated Dopamine D2/3 Receptor Availability in Obese Individuals: A PET Imaging Study with [11C](+)PHNO. Neuropsychopharmacology, 2016, 41, 3042-3050.	2.8	47
123	Receptor Occupancy of the Â-Opioid Antagonist LY2456302 Measured with Positron Emission Tomography and the Novel Radiotracer 11C-LY2795050. Journal of Pharmacology and Experimental Therapeutics, 2016, 356, 260-266.	1.3	47
124	PET imaging of α7 nicotinic acetylcholine receptors: a comparative study of [18F]ASEM and [18F]DBT-10 in nonhuman primates, and further evaluation of [18F]ASEM in humans. European Journal of Nuclear Medicine and Molecular Imaging, 2017, 44, 1042-1050.	3.3	47
125	Metabotropic Glutamate Receptor 5 and Glutamate Involvement in Major Depressive Disorder: A Multimodal Imaging Study. Biological Psychiatry: Cognitive Neuroscience and Neuroimaging, 2017, 2, 449-456.	1.1	47
126	Guidelines for the content and format of PET brain data in publications and archives: A consensus paper. Journal of Cerebral Blood Flow and Metabolism, 2020, 40, 1576-1585.	2.4	47

#	Article	IF	CITATIONS
127	InÂVivo Reactive Oxygen Species Detection With a Novel Positron Emission Tomography Tracer, 18F-DHMT, Allows for Early Detection of Anthracycline-Induced Cardiotoxicity in Rodents. JACC Basic To Translational Science, 2018, 3, 378-390.	1.9	46
128	Radiolabeling of Poly(lactic- <i>co</i> -glycolic acid) (PLGA) Nanoparticles with Biotinylated F-18 Prosthetic Groups and Imaging of Their Delivery to the Brain with Positron Emission Tomography. Bioconjugate Chemistry, 2014, 25, 2157-2165.	1.8	45
129	A singleâ€center, openâ€label positron emission tomography study to evaluate brivaracetam and levetiracetam synaptic vesicle glycoprotein 2A binding in healthy volunteers. Epilepsia, 2019, 60, 958-967.	2.6	45
130	Assessment of population-based input functions for Patlak imaging of whole body dynamic 18F-FDG PET. EJNMMI Physics, 2020, 7, 67.	1.3	45
131	Brain Uptake of the Acid Metabolites of F-18—Labeled WAY 100635 Analogs. Journal of Cerebral Blood Flow and Metabolism, 2003, 23, 249-260.	2.4	44
132	Evaluation of <sup>11</sup> C-BU99008, a PET Ligand for the Imidazoline <sub>2</sub> Binding Sites in Rhesus Brain. Journal of Nuclear Medicine, 2014, 55, 838-844.	2.8	44
133	PET Imaging for Early Detection of Alzheimer's Disease. PET Clinics, 2017, 12, 329-350.	1.5	44
134	Data-driven event-by-event respiratory motion correction using TOF PET list-mode centroid of distribution. Physics in Medicine and Biology, 2017, 62, 4741-4755.	1.6	44
135	Imaging Nicotine- and Amphetamine-Induced Dopamine Release in Rhesus Monkeys with [11C]PHNO vs [11C]raclopride PET. Neuropsychopharmacology, 2014, 39, 866-874.	2.8	43
136	Age-related changes in binding of the D2/3 receptor radioligand [11C](+)PHNO in healthy volunteers. NeuroImage, 2016, 130, 241-247.	2.1	43
137	Dose-Related Target Occupancy and Effects on Circuitry, Behavior, and Neuroplasticity of the Glycine Transporter-1 Inhibitor PF-03463275 in Healthy and Schizophrenia Subjects. Biological Psychiatry, 2018, 84, 413-421.	0.7	43
138	Parametric Imaging With PET and SPECT. IEEE Transactions on Radiation and Plasma Medical Sciences, 2020, 4, 1-23.	2.7	43
139	Comparison of [ <sup>11</sup> C]UCB-J and [ <sup>18</sup> F]FDG PET in Alzheimer's disease: A tracer kinetic modeling study. Journal of Cerebral Blood Flow and Metabolism, 2021, 41, 2395-2409.	2.4	43
140	A Statistical Model for Positron Emission Tomography: Comment. Journal of the American Statistical Association, 1985, 80, 20.	1.8	42
141	Measurement of Regional Rates of Cerebral Protein Synthesis with L-[1-11C]leucine and PET with Correction for Recycling of Tissue Amino Acids: II. Validation in Rhesus Monkeys. Journal of Cerebral Blood Flow and Metabolism, 2005, 25, 629-640.	2.4	42
142	Radiosynthesis and in vivo evaluation of [11C]MP-10 as a positron emission tomography radioligand for phosphodiesterase 10A. Nuclear Medicine and Biology, 2011, 38, 875-884.	0.3	42
143	Direct 4-D PET List Mode Parametric Reconstruction With a Novel EM Algorithm. IEEE Transactions on Medical Imaging, 2012, 31, 2213-2223.	5.4	42
144	Studies of the metabotropic glutamate receptor 5 radioligand [ <sup>11</sup> C]ABP688 with <i>N</i> -acetylcysteine challenge in rhesus monkeys. Synapse, 2013, 67, 489-501.	0.6	42

#	Article	IF	CITATIONS
145	Kinetic Modeling of 11C-LY2795050, A Novel Antagonist Radiotracer for PET Imaging of the Kappa Opioid Receptor in Humans. Journal of Cerebral Blood Flow and Metabolism, 2014, 34, 1818-1825.	2.4	42
146	Task-Related Interaction between Basal Ganglia and Cortical Dopamine Release. Journal of Neuroscience, 2007, 27, 14434-14441.	1.7	41
147	Decreased norepinephrine transporter availability in obesity: Positron Emission Tomography imaging with (S,S)-[11C]O-methylreboxetine. NeuroImage, 2014, 86, 306-310.	2.1	41
148	High-resolution imaging of brain 5-HT1B receptors in the rhesus monkey using [11C]P943. Nuclear Medicine and Biology, 2010, 37, 205-214.	0.3	40
149	Imaging signal transduction via arachidonic acid in the human brain during visual stimulation, by means of positron emission tomography. NeuroImage, 2007, 34, 1342-1351.	2.1	39
150	Event-by-Event Continuous Respiratory Motion Correction for Dynamic PET Imaging. Journal of Nuclear Medicine, 2016, 57, 1084-1090.	2.8	39
151	Microglial depletion and activation: A [11C]PBR28 PET study in nonhuman primates. EJNMMI Research, 2017, 7, 59.	1.1	39
152	Parametric Imaging and Test–Retest Variability of <sup>11</sup> C-(+)-PHNO Binding to D <sub>2</sub> /D <sub>3</sub> Dopamine Receptors in Humans on the High-Resolution Research Tomograph PET Scanner. Journal of Nuclear Medicine, 2014, 55, 960-966.	2.8	38
153	OCD is associated with an altered association between sensorimotor gating and cortical and subcortical 5-HT1b receptor binding. Journal of Affective Disorders, 2016, 196, 87-96.	2.0	38
154	Synthesis and in vivo evaluation of [18F]UCB-J for PET imaging of synaptic vesicle glycoprotein 2A (SV2A). European Journal of Nuclear Medicine and Molecular Imaging, 2019, 46, 1952-1965.	3.3	38
155	Reversal of synapse loss in Alzheimer mouse models by targeting mGluR5 to prevent synaptic tagging by C1Q. Science Translational Medicine, 2022, 14, .	5.8	38
156	Brain Serotonin Synthesis Rates in Rhesus Monkeys Determined by [11C]α-Methyl-?-Tryptophan and Positron Emission Tomography Compared to CSF 5-Hydroxyindole-3-Acetic Acid Concentrations. Neuropsychopharmacology, 1998, 19, 345-353.	2.8	37
157	Test–retest reproducibility of the metabotropic glutamate receptor 5 ligand [18F]FPEB with bolus plus constant infusion in humans. European Journal of Nuclear Medicine and Molecular Imaging, 2015, 42, 1530-1541.	3.3	37
158	High Single Doses of Radiation May Induce Elevated Levels of Hypoxia in Early-Stage Non-Small Cell Lung Cancer Tumors. International Journal of Radiation Oncology Biology Physics, 2018, 102, 174-183.	0.4	36
159	Kappa-opioid receptors, dynorphin, and cocaine addiction: a positron emission tomography study. Neuropsychopharmacology, 2019, 44, 1720-1727.	2.8	36
160	Test–Retest Reproducibility of Binding Parameters in Humans with <sup>11</sup> C-LY2795050, an Antagonist PET Radiotracer for the κ Opioid Receptor. Journal of Nuclear Medicine, 2015, 56, 243-248.	2.8	35
161	First-in-Human Assessment of <sup>11</sup> C-LSN3172176, an M1 Muscarinic Acetylcholine Receptor PET Radiotracer. Journal of Nuclear Medicine, 2021, 62, 553-560.	2.8	35
162	Precision and Accuracy Considerations of Physiological Quantitation in PET. Journal of Cerebral Blood Flow and Metabolism, 1991, 11, A45-A50.	2.4	34

#	Article	IF	CITATIONS
163	Determination of the In Vivo Selectivity of a New κ-Opioid Receptor Antagonist PET Tracer <sup>11</sup> C-LY2795050 in the Rhesus Monkey. Journal of Nuclear Medicine, 2013, 54, 1668-1674.	2.8	34
164	Quantification of myocardial blood flow with 82Rb: Validation with 15O-water using time-of-flight and point-spread-function modeling. EJNMMI Research, 2016, 6, 68.	1.1	34
165	Age-Related Change in 5-HT <sub>6</sub> Receptor Availability in Healthy Male Volunteers Measured with <sup>11</sup> C-GSK215083 PET. Journal of Nuclear Medicine, 2018, 59, 1445-1450.	2.8	34
166	In vivo evidence for dysregulation of mGluR5 as a biomarker of suicidal ideation. Proceedings of the National Academy of Sciences of the United States of America, 2019, 116, 11490-11495.	3.3	34
167	Synthesis and Preclinical Evaluation of an <sup>18</sup> F-Labeled Synaptic Vesicle Glycoprotein 2A PET Imaging Probe: [ <sup>18</sup> F]SynVesT-2. ACS Chemical Neuroscience, 2020, 11, 592-603.	1.7	34
168	Quantification of Smoking-Induced Occupancy of β2-Nicotinic Acetylcholine Receptors: Estimation of Nondisplaceable Binding. Journal of Nuclear Medicine, 2010, 51, 1226-1233.	2.8	33
169	Imaging Changes in Synaptic Acetylcholine Availability in Living Human Subjects. Journal of Nuclear Medicine, 2013, 54, 78-82.	2.8	33
170	Non-Rigid Event-by-Event Continuous Respiratory Motion Compensated List-Mode Reconstruction for PET. IEEE Transactions on Medical Imaging, 2018, 37, 504-515.	5.4	33
171	Brain Glucose Metabolism in Noninsulin-Dependent Diabetes Mellitus: A Study in Pima Indians Using Positron Emission Tomography during Hyperinsulinemia with Euglycemic Glucose Clamp. Journal of Clinical Endocrinology and Metabolism, 1990, 71, 1602-1610.	1.8	32
172	Regional and source-based patterns of [ 11 C]-(+)-PHNO binding potential reveal concurrent alterations in dopamine D 2 and D 3 receptor availability in cocaine-use disorder. NeuroImage, 2017, 148, 343-351.	2.1	32
173	Data-driven voluntary body motion detection and non-rigid event-by-event correction for static and dynamic PET. Physics in Medicine and Biology, 2019, 64, 065002.	1.6	32
174	Preliminary in vivo evidence of lower hippocampal synaptic density in cannabis use disorder. Molecular Psychiatry, 2021, 26, 3192-3200.	4.1	32
175	Data-Driven Motion Detection and Event-by-Event Correction for Brain PET: Comparison with Vicra. Journal of Nuclear Medicine, 2020, 61, 1397-1403.	2.8	32
176	Multiple-Radionuclide Autoradiography in Evaluation of Cerebral Function. Journal of Cerebral Blood Flow and Metabolism, 1984, 4, 264-269.	2.4	31
177	Ex Vivo and In Vivo Evaluation of the Norepinephrine Transporter Ligand [11C]MRB for Brown Adipose Tissue Imaging. Nuclear Medicine and Biology, 2012, 39, 1081-1086.	0.3	31
178	Determination of In Vivo <i>B</i> <sub>max</sub> and <i>K</i> <sub>d</sub> for <sup>11</sup> C-GR103545, an Agonist PET Tracer for κ-Opioid Receptors: A Study in Nonhuman Primates. Journal of Nuclear Medicine, 2013, 54, 600-608.	2.8	31
179	Determination of receptor occupancy in the presence of mass dose: [11C]GSK189254 PET imaging of histamine H3 receptor occupancy by PF-03654746. Journal of Cerebral Blood Flow and Metabolism, 2017, 37, 1095-1107.	2.4	31
180	In vivo muscarinic binding of 3-(alkylthio)-3-thiadiazolyl tetrahydropyridines. Synapse, 1999, 31, 29-40.	0.6	30

#	Article	IF	CITATIONS
181	Reduced post-synaptic serotonin type 1A receptor binding in bipolar depression. European Neuropsychopharmacology, 2013, 23, 822-829.	0.3	30
182	Experimentally reducing corticosterone mitigates rapid captivity effects on behavior, but not body composition, in a wild bird. Hormones and Behavior, 2017, 89, 121-129.	1.0	29
183	PET imaging of mGluR5 in Alzheimer's disease. Alzheimer's Research and Therapy, 2020, 12, 15.	3.0	29
184	Imaging of Synaptic Density in Neurodegenerative Disorders. Journal of Nuclear Medicine, 2022, 63, 60S-67S.	2.8	29
185	Cortical β-amyloid burden, gray matter, and memory in adults at varying APOE ε4 risk for Alzheimer's disease. Neurobiology of Aging, 2018, 61, 207-214.	1.5	28
186	Binding of the synaptic vesicle radiotracer [ <sup>11</sup> C]UCB-J is unchanged during functional brain activation using a visual stimulation task. Journal of Cerebral Blood Flow and Metabolism, 2021, 41, 1067-1079.	2.4	28
187	Differential effects of paroxetine on raphe and cortical 5-HT1A binding: A PET study in monkeys. NeuroImage, 2005, 28, 238-248.	2.1	27
188	Eventâ€byâ€event respiratory motion correction for PET with 3D internal″D external motion correlation. Medical Physics, 2013, 40, 112507.	1.6	27
189	First-in-Human Assessment of the Novel PDE2A PET Radiotracer <sup>18</sup> F-PF-05270430. Journal of Nuclear Medicine, 2016, 57, 1388-1395.	2.8	27
190	Brain Incorporation of [11C]Arachidonic Acid in Young Healthy Humans Measured With Positron Emission Tomography. Journal of Cerebral Blood Flow and Metabolism, 2002, , 1453-1462.	2.4	27
191	Hyperosmolar blood-brain barrier disruption in baboons: an in vivo study using positron emission tomography and rubidium-82. Journal of Neurosurgery, 1996, 84, 494-502.	0.9	26
192	Age Effects on Serotonin Receptor 1B as Assessed by PET. Journal of Nuclear Medicine, 2012, 53, 1411-1414.	2.8	26
193	Optimization of PET–MR registrations for nonhuman primates using mutual information measures: A Multi-Transform Method (MTM). NeuroImage, 2013, 64, 571-581.	2.1	26
194	An Improved Antagonist Radiotracer for the κ-Opioid Receptor: Synthesis and Characterization of 11C-LY2459989. Journal of Nuclear Medicine, 2014, 55, 1185-1191.	2.8	26
195	Kappa opioid receptor binding in major depression: A pilot study. Synapse, 2018, 72, e22042.	0.6	26
196	Imaging human brown adipose tissue under room temperature conditions with 11C-MRB, a selective norepinephrine transporter PET ligand. Metabolism: Clinical and Experimental, 2015, 64, 747-755.	1.5	25
197	A preliminary study of dopamine D2/3 receptor availability and social status in healthy and cocaine dependent humans imaged with [11C](+)PHNO. Drug and Alcohol Dependence, 2015, 154, 167-173.	1.6	25
198	Preliminary In Vivo Evidence of Reduced Synaptic Density in Human Immunodeficiency Virus (HIV) Despite Antiretroviral Therapy. Clinical Infectious Diseases, 2021, 73, 1404-1411.	2.9	25

#	Article	IF	CITATIONS
199	Association of entorhinal cortical tau deposition and hippocampal synaptic density in older individuals with normal cognition and early Alzheimer's disease. Neurobiology of Aging, 2022, 111, 44-53.	1.5	25
200	lmaging the effect of ketamine on synaptic density (SV2A) in the living brain. Molecular Psychiatry, 2022, 27, 2273-2281.	4.1	25
201	Dopamine D3 receptor antagonists: The quest for a potentially selective PET ligand. Part 3: Radiosynthesis and in vivo studies. Bioorganic and Medicinal Chemistry Letters, 2009, 19, 5056-5059.	1.0	24
202	Evaluation of Pancreatic VMAT2 Binding with Active and Inactive Enantiomers of [18F]FP-DTBZ in Healthy Subjects and Patients with Type 1 Diabetes. Molecular Imaging and Biology, 2018, 20, 835-845.	1.3	24
203	Determination of [18F]FCWAY, [18F]FP-TZTP, and their metabolites in plasma using rapid and efficient liquid-liquid and solid phase extractions. Nuclear Medicine and Biology, 2003, 30, 233-240.	0.3	23
204	A Potential Cholinergic Mechanism of Procaine's Limbic Activation. Neuropsychopharmacology, 2004, 29, 1239-1250.	2.8	23
205	Noradrenergic Activity in the Human Brain: A Mechanism Supporting the Defense Against Hypoglycemia. Journal of Clinical Endocrinology and Metabolism, 2018, 103, 2244-2252.	1.8	23
206	Assessment of test-retest reproducibility of [18F]SynVesT-1, a novel radiotracer for PET imaging of synaptic vesicle glycoprotein 2A. European Journal of Nuclear Medicine and Molecular Imaging, 2021, 48, 1327-1338.	3.3	23
207	Optimization of Noninvasive Activation Studies with 15O-Water and Three-Dimensional Positron Emission Tomography. Journal of Cerebral Blood Flow and Metabolism, 1997, 17, 732-739.	2.4	22
208	Count-Rate Dependent Component-Based Normalization for the HRRT. IEEE Transactions on Nuclear Science, 2007, 54, 486-495.	1.2	22
209	Evaluation of PET Brain Radioligands for Imaging Pancreatic β-Cell Mass: Potential Utility of 11C-(+)-PHNO. Journal of Nuclear Medicine, 2018, 59, 1249-1254.	2.8	22
210	Social status and demographic effects of the kappa opioid receptor: a PET imaging study with a novel agonist radiotracer in healthy volunteers. Neuropsychopharmacology, 2019, 44, 1714-1719.	2.8	22
211	Assessing the sensitivity of [ <sup>11</sup> C]p943, a novel 5â€HT <sub>IB</sub> radioligand, to endogenous serotonin release. Synapse, 2011, 65, 1113-1117.	0.6	21
212	Tobacco smoking interferes with GABA <sub>A</sub> receptor neuroadaptations during prolonged alcohol withdrawal. Proceedings of the National Academy of Sciences of the United States of America, 2014, 111, 18031-18036.	3.3	21
213	Evaluation of the sensitivity of the novel α4β2* nicotinic acetylcholine receptor PET radioligand <sup>18</sup> Fâ€{â€}â€NCFHEB to increases in synaptic acetylcholine levels in rhesus monkeys. Synapse, 2014, 68, 556-564.	0.6	21
214	Quantitative PET Imaging in Drug Development: Estimation of Target Occupancy. Bulletin of Mathematical Biology, 2019, 81, 3508-3541.	0.9	21
215	Test–retest reliability of the novel 5-HT1B receptor PET radioligand [11C]P943. European Journal of Nuclear Medicine and Molecular Imaging, 2015, 42, 468-477.	3.3	20
216	Evaluation of pancreatic VMAT2 binding with active and inactive enantiomers of 18 F-FP-DTBZ in baboons. Nuclear Medicine and Biology, 2016, 43, 743-751.	0.3	20

#	Article	IF	CITATIONS
217	PET imaging evaluation of [18F]DBT-10, a novel radioligand specific to α7 nicotinic acetylcholine receptors, in nonhuman primates. European Journal of Nuclear Medicine and Molecular Imaging, 2016, 43, 537-547.	3.3	20
218	Quantification of SV2A Binding in Rodent Brain Using [18F]SynVesT-1 and PET Imaging. Molecular Imaging and Biology, 2021, 23, 372-381.	1.3	20
219	PET-BIDS, an extension to the brain imaging data structure for positron emission tomography. Scientific Data, 2022, 9, 65.	2.4	20
220	Noninvasive Estimation of Normalized Distribution Volume: Application to the Muscarinic-2 Ligand [18F]FP-TZTP. Journal of Cerebral Blood Flow and Metabolism, 2008, 28, 420-430.	2.4	19
221	Direct 4D list mode parametric reconstruction for PET with a novel EM algorithm. , 2008, 4774103, 3625-3628.		19
222	Awake Nonhuman Primate Brain PET Imaging with Minimal Head Restraint: Evaluation of GABA <sub>A</sub> -Benzodiazepine Binding with <sup>11</sup> C-Flumazenil in Awake and Anesthetized Animals. Journal of Nuclear Medicine, 2013, 54, 1962-1968.	2.8	19
223	PET Imaging of Pancreatic Dopamine D <sub>2</sub> and D <sub>3</sub> Receptor Density with <sup>11</sup> C-(+)-PHNO in Type 1 Diabetes. Journal of Nuclear Medicine, 2020, 61, 570-576.	2.8	19
224	Simplified Quantification of <sup>11</sup> C-UCB-J PET Evaluated in a Large Human Cohort. Journal of Nuclear Medicine, 2021, 62, 418-421.	2.8	19
225	Brain Uptake of the Acid Metabolites of F-18???Labeled WAY 100635 Analogs. Journal of Cerebral Blood Flow and Metabolism, 2003, , 249-260.	2.4	19
226	Positron Emission Tomography [150]Water Studies with Short InterScan Interval for Single-Subject and Group Analysis: Influence of Background Subtraction. Journal of Cerebral Blood Flow and Metabolism, 1998, 18, 433-444.	2.4	18
227	Age and APOE-ε4 genotype influence the effect of physostigmine infusion on the in-vivo distribution volume of the muscarinic-2-receptor dependent tracer [18F]FP-TZTP. Synapse, 2006, 60, 86-92.	0.6	18
228	Assessment of a three-dimensional line-of-response probability density function system matrix for PET. Physics in Medicine and Biology, 2012, 57, 6827-6848.	1.6	18
229	Further evaluation of [11C]MP-10 as a radiotracer for phosphodiesterase 10A: PET imaging study in rhesus monkeys and brain tissue metabolite analysis. Synapse, 2015, 69, 86-95.	0.6	18
230	Decreased VMAT2 in the pancreas of humans with type 2 diabetes mellitus measured in vivo by PET imaging. Diabetologia, 2018, 61, 2598-2607.	2.9	18
231	Norepinephrine transporter availability in brown fat is reduced in obesity: a human PET study with [11C] MRB. International Journal of Obesity, 2020, 44, 964-967.	1.6	18
232	Identifying brain networks in synaptic density PET (11C-UCB-J) with independent component analysis. NeuroImage, 2021, 237, 118167.	2.1	18
233	Glia Imaging Differentiates Multiple System Atrophy from Parkinson's Disease: A Positron Emission Tomography Study with [ <scp><sup>11</sup>C</scp> ] <scp>PBR28</scp> and Machine Learning Analysis. Movement Disorders, 2022, 37, 119-129.	2.2	18
234	In vivo muscarinic binding selectivity of QNB. Bioorganic and Medicinal Chemistry, 1997, 5, 1555-1567.	1.4	17

#	Article	IF	CITATIONS
235	Comparison of PET [150]Water Studies with 6-Minute and 10-Minute InterScan Intervals: Single-Subject and Group Analyses. Journal of Cerebral Blood Flow and Metabolism, 1999, 19, 570-582.	2.4	17
236	In Hot Blood. JACC: Cardiovascular Imaging, 2013, 6, 569-573.	2.3	17
237	Tracer Kinetic Modeling of [ <sup>11</sup> C]AFM, a New PET Imaging Agent for the Serotonin Transporter. Journal of Cerebral Blood Flow and Metabolism, 2013, 33, 1886-1896.	2.4	17
238	Evaluation of [ 18 F]-(-)-norchlorofluorohomoepibatidine ([ 18 F]-(-)-NCFHEB) as a PET radioligand to image the nicotinic acetylcholine receptors in non-human primates. Nuclear Medicine and Biology, 2015, 42, 570-577.	0.3	17
239	Quantitative Analysis of Dynamic <sup>123</sup> I-mIBG SPECT Imaging Data in Healthy Humans with a Population-Based Metabolite Correction Method. Journal of Nuclear Medicine, 2016, 57, 1226-1232.	2.8	17
240	Quantification of Tumor Hypoxic Fractions Using Positron Emission Tomography with [18F]Fluoromisonidazole ([18F]FMISO) Kinetic Analysis and Invasive Oxygen Measurements. Molecular Imaging and Biology, 2017, 19, 893-902.	1.3	17
241	Direct reconstruction of parametric images for brain PET with event-by-event motion correction: evaluation in two tracers across count levels. Physics in Medicine and Biology, 2017, 62, 5344-5364.	1.6	17
242	Improved discrimination between benign and malignant LDCT screening-detected lung nodules with dynamic over static <sup>18</sup> F-FDG PET as a function of injected dose. Physics in Medicine and Biology, 2018, 63, 175015.	1.6	17
243	Brain-Dedicated Emission Tomography Systems: A Perspective on Requirements for Clinical Research and Clinical Needs in Brain Imaging. IEEE Transactions on Radiation and Plasma Medical Sciences, 2019, 3, 254-261.	2.7	17
244	Evaluation of <sup>11</sup> C-LSN3172176 as a Novel PET Tracer for Imaging M <sub>1</sub> Muscarinic Acetylcholine Receptors in Nonhuman Primates. Journal of Nuclear Medicine, 2019, 60, 1147-1153.	2.8	17
245	In vivo 5-HT6 and 5-HT2A receptor availability in antipsychotic treated schizophrenia patients vs. unmedicated healthy humans measured with [11C]GSK215083 PET. Psychiatry Research - Neuroimaging, 2020, 295, 111007.	0.9	17
246	Partial volume correction analysis for 11C-UCB-J PET studies of Alzheimer's disease. NeuroImage, 2021, 238, 118248.	2.1	17
247	Evaluation of the Lysophosphatidic Acid Receptor Type 1 Radioligand <sup>11</sup> C-BMT-136088 for Lung Imaging in Rhesus Monkeys. Journal of Nuclear Medicine, 2018, 59, 327-333.	2.8	16
248	Generation of parametric <i>K</i> <sub>i</sub> images for FDG PET using two 5â€min scans. Medical Physics, 2021, 48, 5219-5231.	1.6	16
249	Estradiol modulates neural response to conspecific and heterospecific song in female house sparrows: An in vivo positron emission tomography study. PLoS ONE, 2017, 12, e0182875.	1.1	16
250	A metabolically stable PET tracer for imaging synaptic vesicle protein 2A: synthesis and preclinical characterization of [18F]SDM-16. European Journal of Nuclear Medicine and Molecular Imaging, 2022, 49, 1482-1496.	3.3	16
251	Lower prefrontal cortical synaptic vesicle binding in cocaine use disorder: An exploratory <sup>11</sup> Câ€UCBâ€J positron emission tomography study in humans. Addiction Biology, 2022, 27, e13123.	1.4	16
252	Opiate receptor avidity is reduced in non-motor impaired MPTP-lesioned rhesus monkeys. Brain Research, 1998, 806, 292-296.	1.1	15

#	Article	IF	CITATIONS
253	Atlas-Based Multiorgan Segmentation for Dynamic Abdominal PET. IEEE Transactions on Radiation and Plasma Medical Sciences, 2020, 4, 50-62.	2.7	14
254	Multimodal investigation of dopamine D2/D3 receptors, default mode network suppression, and cognitive control in cocaine-use disorder. Neuropsychopharmacology, 2021, 46, 316-324.	2.8	14
255	Opiate receptor avidity in the thalamus is sexually dimorphic in the elderly. Synapse, 2000, 38, 226-229.	0.6	13
256	Synthesis and evaluation of an 18F analog of forskolin for imaging adenylyl cyclase. Journal of Fluorine Chemistry, 2000, 101, 297-304.	0.9	13
257	Quantitative accuracy of HRRT IIST-MODE reconstructions: Effect of low statistics. , 2008, 2008, 5121-5124.		13
258	Kinetic Analysis of Drug–Target Interactions with PET for Characterization of Pharmacological Hysteresis. Journal of Cerebral Blood Flow and Metabolism, 2013, 33, 700-707.	2.4	13
259	Preclinical Evaluation of <sup>18</sup> F-PF-05270430, a Novel PET Radioligand for the Phosphodiesterase 2A Enzyme. Journal of Nuclear Medicine, 2016, 57, 1448-1453.	2.8	13
260	Measuring the effects of ketamine on mGluR5 using [ <sup>18</sup> F]FPEB and PET. Journal of Cerebral Blood Flow and Metabolism, 2020, 40, 2254-2264.	2.4	13
261	Test-retest reproducibility of [11C]-(+)-propyl-hexahydro-naphtho-oxazin positron emission tomography using the bolus plus constant infusion paradigm. Molecular Imaging, 2013, 12, 77-82.	0.7	13
262	A Realistic Computer-Simulated Brain Phantom for Evaluation of PET Charactenstics. IEEE Transactions on Medical Imaging, 1987, 6, 250-257.	5.4	12
263	Using single photon emission tomography (SPECT) and positron emission tomography (PET) to trace the distribution of muscarinic acetylcholine receptor (MACHR) binding radioligands. Life Sciences, 1999, 64, 511-518.	2.0	12
264	Device-dependent activity estimation and decay correction of radionuclide mixtures with application to Tc-94m PET studies. Medical Physics, 2001, 28, 36-45.	1.6	12
265	Cerebral Metabolic Effects of Intravenous Glycine in Healthy Human Subjects. Journal of Clinical Psychopharmacology, 2006, 26, 595-599.	0.7	12
266	A multimodal approach to image-derived input functions for brain PET. , 2009, 2009, 2710-2714.		12
267	Evaluation of Frame-Based and Event-by-Event Motion-Correction Methods for Awake Monkey Brain PET Imaging. Journal of Nuclear Medicine, 2014, 55, 287-293.	2.8	12
268	[ <sup>11</sup> C]Methionine and [ <sup>11</sup> C]PBR28 as PET Imaging Tracers to Differentiate Metastatic Tumor Recurrence or Radiation Necrosis. Molecular Imaging, 2020, 19, 153601212096866.	0.7	12
269	Generation of synthetic PET images of synaptic density and amyloid from <sup>18</sup> Fâ€FDG images using deep learning. Medical Physics, 2021, 48, 5115-5129.	1.6	12
			-

Amphetamine-Induced Dopamine Release. , 2001, , 205-209.

#	Article	IF	CITATIONS
271	Analysis of Covariance in Statistical Parametric Mapping. Journal of Cerebral Blood Flow and Metabolism, 1993, 13, 1038-1038.	2.4	11
272	Imaging the Enzyme 11β-Hydroxysteroid Dehydrogenase Type 1 with PET: Evaluation of the Novel Radiotracer <sup>11</sup> C-AS2471907 in Human Brain. Journal of Nuclear Medicine, 2019, 60, 1140-1146.	2.8	11
273	Event-by-event non-rigid data-driven PET respiratory motion correction methods: comparison of principal component analysis and centroid of distribution. Physics in Medicine and Biology, 2019, 64, 165014.	1.6	11
274	Opiate receptor avidity is reduced bilaterally in rhesus monkeys unilaterally lesioned with MPTP. , 1999, 33, 282-288.		10
275	Consensus nomenclature: its time has come. European Journal of Nuclear Medicine and Molecular Imaging, 2007, 34, 1239-1239.	3.3	10
276	Measurement of <i>B</i> <sub>max</sub> and <i>K</i> <sub>d</sub> with the Glycine Transporter 1 Radiotracer <sup>18</sup> F-MK6577 using a Novel Multi-Infusion Paradigm. Journal of Cerebral Blood Flow and Metabolism, 2015, 35, 2001-2009.	2.4	10
277	First in-human PET study and kinetic evaluation of [ <sup>18</sup> F]AS2471907 for imaging 11î²-hydroxysteroid dehydrogenase type 1. Journal of Cerebral Blood Flow and Metabolism, 2020, 40, 695-704.	2.4	10
278	Kinetic Modeling and Test–Retest Reproducibility of <sup>11</sup> C-EKAP and <sup>11</sup> C-FEKAP, Novel Agonist Radiotracers for PET Imaging of the lº-Opioid Receptor in Humans. Journal of Nuclear Medicine, 2020, 61, 1636-1642.	2.8	10
279	Effect of age on brain metabotropic glutamate receptor subtype 5 measured with [18F]FPEB PET. NeuroImage, 2021, 238, 118217.	2.1	10
280	PET Imaging of Synaptic Vesicle Protein 2A. , 2021, , 993-1019.		10
281	Imaging brain cortisol regulation in PTSD with a target for 11β-hydroxysteroid dehydrogenase type 1. Journal of Clinical Investigation, 2021, 131, .	3.9	10
282	Bolus Injection versus Slow Infusion of [150]Water for Positron Emission Tomography Activation Studies. Journal of Cerebral Blood Flow and Metabolism, 1999, 19, 843-852.	2.4	9
283	Direct EM reconstruction of kinetic parameters from list-mode cardiac PET. , 2014, , .		9
284	Cardiacâ€gated parametric images from <sup>82</sup> Rb <scp>PET</scp> from dynamic frames and direct 4D reconstruction. Medical Physics, 2018, 45, 639-654.	1.6	9
285	Body Mass Index and Age Effects on Brain 11β-Hydroxysteroid Dehydrogenase Type 1: a Positron Emission Tomography Study. Molecular Imaging and Biology, 2020, 22, 1124-1131.	1.3	9
286	Inverse changes in raphe and cortical 5â€HT 1B receptor availability after acute tryptophan depletion in healthy human subjects. Synapse, 2020, 74, e22159.	0.6	9
287	Separating dopamine D2 and D3 receptor sources of [11C]-(+)-PHNO binding potential: Independent component analysis of competitive binding. NeuroImage, 2020, 214, 116762.	2.1	9
288	Novel Reversible-Binding PET Ligands for Imaging Monoacylglycerol Lipase Based on the Piperazinyl Azetidine Scaffold. Journal of Medicinal Chemistry, 2021, 64, 14283-14298.	2.9	9

#	Article	IF	CITATIONS
289	The Search for a Subtype-Selective PET Imaging Agent for the GABA <sub>A</sub> Receptor Complex: Evaluation of the Radiotracer [ <sup>11</sup> C]ADO in Nonhuman Primates. Molecular Imaging, 2017, 16, 153601211773125.	0.7	8
290	Tobacco Smoking in People Is Not Associated with Altered 18-kDa Translocator Protein Levels: A PET Study. Journal of Nuclear Medicine, 2020, 61, 1200-1204.	2.8	8
291	Human adult and adolescent biodistribution and dosimetry of the synaptic vesicle glycoprotein 2A radioligand 11C-UCB-J. EJNMMI Research, 2020, 10, 83.	1.1	8
292	Characterization in nonhuman primates of (R)-[18F]OF-Me-NB1 and (S)-[18F]OF-Me-NB1 for imaging the GluN2B subunits of the NMDA receptor. European Journal of Nuclear Medicine and Molecular Imaging, 2022, , 1.	3.3	8
293	Adaptive data-driven motion detection and optimized correction for brain PET. Neurolmage, 2022, 252, 119031.	2.1	8
294	Initial evaluation of direct 4D parametric reconstruction with human PET data. , 2009, 2009, 2503-2506.		7
295	962. In-vivo Evidence of Decreased Synaptic Density in Schizophrenia: A [11C]UCB-J PET Imaging Study. Biological Psychiatry, 2017, 81, S389.	0.7	7
296	Evaluation of (â€)â€{ <sup>18</sup> <scp>F]F</scp> lubatineâ€specific binding: Implications for reference region approaches. Synapse, 2018, 72, e22016.	0.6	7
297	Direct List Mode Parametric Reconstruction for Dynamic Cardiac SPECT. IEEE Transactions on Medical Imaging, 2020, 39, 119-128.	5.4	7
298	Longitudinal imaging of metabotropic glutamate 5 receptors during early and extended alcohol abstinence. Neuropsychopharmacology, 2021, 46, 380-385.	2.8	7
299	Lower synaptic density is associated with psychiatric and cognitive alterations in obesity. Neuropsychopharmacology, 2021, , .	2.8	7
300	Imaging Pituitary Vasopressin 1B Receptor in Humans with the PET Radiotracer <sup>11</sup> C-TASP699. Journal of Nuclear Medicine, 2022, 63, 609-614.	2.8	7
301	Absolute Cerebral Blood Flow with [150]Water and PET. , 1996, , 185-190.		7
302	Comparison of three novel radiotracers for GluN2B-containing NMDA receptors in non-human primates: <i>(R)</i> -[ <sup>11</sup> C]NR2B-Me, <i>(R)</i> -[ <sup>18</sup> F]of-Me-NB1, and <i>(S)</i> -[ <sup>18</sup> F]of-NB1. Journal of Cerebral Blood Flow and Metabolism, 2022, 42, 1398-1409.	2.4	7
303	Cerebral blood flow in temporal lobe epilepsy: a partial volume correction study. European Journal of Nuclear Medicine and Molecular Imaging, 2007, 34, 2066-2072.	3.3	6
304	Accuracy of head motion compensation for the HRRT: Comparison of methods. , 2009, 2009, 3199-3202.		6
305	Count-rate dependent resolution degradation from pulse pile-up on the HRRT. , 2010, , .		6
306	Investigation of Sub-Centimeter Lung Nodule Quantification for Low-Dose PET. IEEE Transactions on Radiation and Plasma Medical Sciences, 2018, 2, 41-50.	2.7	6

#	Article	IF	CITATIONS
307	A 3D-printed modular device for imaging the brain of small birds. Journal of Neuroscience Methods, 2018, 293, 183-190.	1.3	6
308	Clinical and scientific value in the pursuit of quantification of beta cells in the pancreas by PET imaging. Diabetologia, 2018, 61, 2671-2673.	2.9	6
309	Quantification of PET infusion studies without true equilibrium: A tissue clearance correction. Journal of Cerebral Blood Flow and Metabolism, 2020, 40, 860-874.	2.4	6
310	Acute neuroimmune stimulation impairs verbal memory in adults: A PET brain imaging study. Brain, Behavior, and Immunity, 2021, 91, 784-787.	2.0	6
311	Synthesizing Multi-tracer PET Images for Alzheimer's Disease Patients Using a 3D Unified Anatomy-Aware Cyclic Adversarial Network. Lecture Notes in Computer Science, 2021, , 34-43.	1.0	6
312	A kinetic comparison of [18F]2-fluoro-2-deoxyglucose and [18F]2-fluoro-2-deoxymannose using positron emission tomography. Nuclear Medicine and Biology, 1994, 21, 857-863.	0.3	5
313	Axial slice width in 3D PET: characterization and potential improvement with axial interleaving. Physics in Medicine and Biology, 1998, 43, 921-928.	1.6	5
314	Event-by-event respiratory motion correction for PET with 3-Dimensional internal-external motion correlation. , 2012, , .		5
315	Nicotine and Nicotine Abstinence Do Not Interfere with GABA <sub>A</sub> Receptor Neuroadaptations During Alcohol Abstinence. Alcoholism: Clinical and Experimental Research, 2016, 40, 698-705.	1.4	5
316	Quantitative projection of human brain penetration of the H <sub>3</sub> antagonist PF-03654746 by integrating rat-derived brain partitioning and PET receptor occupancy. Xenobiotica, 2017, 47, 119-126.	0.5	5
317	Simplified Quantification and Acquisition Protocol for <sup>123</sup> I-MIBG Dynamic SPECT. Journal of Nuclear Medicine, 2018, 59, 1574-1580.	2.8	5
318	Feasibility study of PET dynamic imaging of [18F]DHMT for quantification of reactive oxygen species in the myocardium of large animals. Journal of Nuclear Cardiology, 2022, 29, 216-225.	1.4	5
319	PET Imaging Estimates of Regional Acetylcholine Concentration Variation in Living Human Brain. Cerebral Cortex, 2021, 31, 2787-2798.	1.6	5
320	PET Imaging of Synaptic Density: Challenges and Opportunities of Synaptic Vesicle Glycoprotein 2A PET in Small Animal Imaging. Frontiers in Neuroscience, 2022, 16, 787404.	1.4	5
321	Opiate receptor avidity is increased in rhesus monkeys following unilateral optic tract lesion combined with transections of corpus callosum and hippocampal and anterior commissures. Brain Research, 2000, 879, 1-6.	1.1	4
322	Direct, Quantitative, and Noninvasive Imaging of the Transport of Active Agents Through Intact Brain with Positron Emission Tomography. Molecular Imaging and Biology, 2013, 15, 596-605.	1.3	4
323	Comparative evaluation of two glycine transporter 1 radiotracers [11C]GSK931145 and [18F]MK-6577 in baboons. Synapse, 2016, 70, 112-120.	0.6	4
324	F149. Preliminary Evidence for Altered Synaptic Density and a Possible Role for Accelerated Ageing in Individuals With MDD as Measured With [11C]UCB-J PET. Biological Psychiatry, 2018, 83, S296.	0.7	4

#	Article	IF	CITATIONS
325	142. Synaptic Density Alterations are Associated With Depression Severity and Network Alterations. Biological Psychiatry, 2019, 85, S59.	0.7	4
326	Imaging the fetal nonhuman primate brain with SV2A positron emission tomography (PET). European Journal of Nuclear Medicine and Molecular Imaging, 2022, 49, 3679-3691.	3.3	4
327	III. Biomathematical Aspects of Physiological Brain Imaging. Journal of Cerebral Blood Flow and Metabolism, 1987, 7, S11-S13.	2.4	3
328	Validation of the spatially variant probability density functions for the HRRT. , 2011, , .		3
329	List-mode reconstruction for the Biograph mCT with probabilistic line-of-response positioning and event-by-event motion correction. , 2012, , .		3
330	Data-driven respiratory motion estimation and correction using TOF PET list-mode centroid of distribution. , 2014, , .		3
331	Assessment of kinetic modeling quality of fit by cluster analysis of residuals: Application to direct reconstruction of cardiac PET data. , 2015, , .		3
332	Direct EM reconstruction of parametric images from list-mode brain PET using a novel model based on logan graphical analysis. , 2016, , .		3
333	389. In Vivo Evidence of Lower Synaptic Density in Depression and Associated Mood and Cognitive Deficits: A [11C]UCB-J PET Imaging Study. Biological Psychiatry, 2017, 81, S159.	0.7	3
334	Initial Experience with PET Imaging of Synaptic Density (SV2A) in Alzheimer's Disease: A New Biomarker for Clinical Trials?. American Journal of Geriatric Psychiatry, 2018, 26, S145-S146.	0.6	3
335	In vivo imaging of D2 receptors and corticosteroids predict behavioural responses to captivity stress in a wild bird. Scientific Reports, 2019, 9, 10407.	1.6	3
336	ICAâ€derived sources of synaptic density PET ([ 11 C]UCBâ€J) relate to cognitive impairment severity in Alzheimer's disease. Alzheimer's and Dementia, 2020, 16, e041197.	0.4	3
337	Multiparametric cardiac 18F-FDG PET in humans: pilot comparison of FDG delivery rate with 82Rb myocardial blood flow. Physics in Medicine and Biology, 2021, 66, 155015.	1.6	3
338	Scatchard Analysis with Bolus/Infusion Administration of [11C]Raclopride. , 2002, , 63-69.		3
339	Feasibility of imaging synaptic density in the human spinal cord using [11C]UCB-J PET. EJNMMI Physics, 2022, 9, 32.	1.3	3
340	Theoretical Analysis of Optimal Conditions in Fquilibrium Imaging of in Vivo Receptors. IEEE Transactions on Nuclear Science, 1985, 32, 1496-1502.	1.2	2
341	Multiple acquisition frame-based motion correction for awake monkey PET imaging. , 2010, , .		2
342	Kinetic analysis of the kappa agonist tracer [11C]GR103545 in healthy controls. NeuroImage, 2010, 52, S172.	2.1	2

#	Article	IF	CITATIONS
343	Abdominal multi-organ segmentation of dynamic PET studies using modified fuzzy clustering algorithm. , 2015, , .		2
344	Trends in Radiation Medical Sciences: Instrumentation and Imaging Algorithms. IEEE Transactions on Radiation and Plasma Medical Sciences, 2017, 1, 201-205.	2.7	2
345	F188. Preliminary Evidence for mGluR5 Dysregulation in Borderline Personality Disorder and Relationship to Suicidal Behavior. Biological Psychiatry, 2018, 83, S312.	0.7	2
346	Association between cerebrospinal fluid biomarkers of neurodegeneration and PET measurements of synaptic density in Alzheimer's disease. Alzheimer's and Dementia, 2020, 16, e044211.	0.4	2
347	Optimized Methodology for Reference Region and Image-Derived Input Function Kinetic Modeling in Preclinical PET. IEEE Transactions on Radiation and Plasma Medical Sciences, 2022, 6, 454-462.	2.7	2
348	Tracer Kinetic Modeling in Positron Computed Tomography. Lecture Notes in Biomathematics, 1983, , 298-344.	0.3	2
349	An Efficient Algorithm for Reconsiruction of SPECT Images in the Presence of Spatially Varying Attenuation. IEEE Transactions on Nuclear Science, 1985, 32, 1190-1197.	1.2	1
350	Evaluation of direct 4D parametric reconstruction with low count human PET data. , 2010, , .		1
351	Kinetic modeling of the mGluR5 tracer [18F]F-FPEB in humans. NeuroImage, 2010, 52, S169-S170.	2.1	1
352	Awake nonhuman primate brain PET imaging without head restraint. Neurolmage, 2010, 52, S18.	2.1	1
353	Myocardial blood flow from dynamic PET using Independent Component Analysis. , 2012, , .		1
354	Uniform Spatial resolution list mode reconstruction for the HRRT. , 2012, , .		1
355	Effect of subsets on bias and variance in low-count iterative PET reconstruction. , 2013, , .		1
356	Accounting for Breathing Pattern Variability in Event-by-Event Respiratory Motion Correction in PET Using Dynamic Internal-External Motion Correlation. , 2017, , .		1
357	GPU-based List-mode Direct Parametric Reconstruction for Dynamic Cardiac SPECT. , 2017, , .		1
358	P1â€469: PET IMAGING OF METABOTROPIC GLUTAMATE RECEPTOR 5 BINDING IN ALZHEIMER'S DISEASE. Alzheimer's and Dementia, 2018, 14, P501.	0.4	1
359	REGION-SPECIFIC ATROPHY AS MEASURED BY CORTICAL GRAY MATTER VOLUME IS ASSOCIATED WITH BOTH REGIONAL AND TOTAL CORTICAL AMYLOID-BETA BURDEN IN COGNITIVELY NORMAL INDIVIDUALS AT RISK FOR ALZHEIMER'S DISEASE. American Journal of Geriatric Psychiatry, 2019, 27, S186-S187.	0.6	1
360	The rate of dasotraline brain entry is slow following intravenous administration. Psychopharmacology, 2020, 237, 3435-3446.	1.5	1

#	Article	IF	CITATIONS
361	In vivo measurement of widespread synaptic loss and associated tau accumulation in early Alzheimer's disease. Alzheimer's and Dementia, 2020, 16, e037791.	0.4	1
362	Validation of a simplified tissueâ€toâ€teference ratio measurement using SUVR for the assessment of synaptic density alterations in Alzheimer's disease using [ 11 C]UCBâ€J PET. Alzheimer's and Dementia, 2020, 16, e045928.	0.4	1
363	Dopamine D2/3 receptor availability in cocaine use disorder individuals with obesity as measured by [11C]PHNO PET. Drug and Alcohol Dependence, 2021, 220, 108514.	1.6	1
364	[α-11C]Methyl-l-tryptophan in Anesthetized Rhesus Monkeys. , 2001, , 229-235.		1
365	Quantitative Cerebral Blood Flow with PET in the 1980s: Going with the Flow (perspective on a eceBrain) IJ ETQq.	2.8	1 1
366	Dournar of Nuclear Medicine, 2020, 61, 895-0045. Data-driven analysis of kappa opioid receptor binding in major depressive disorder measured by positron emission tomography. Translational Psychiatry, 2021, 11, 602.	2.4	1
367	Target occupancy study and whole-body dosimetry with a MAGL PET ligand [11C]PF-06809247 in non-human primates. EJNMMI Research, 2022, 12, 13.	1.1	1
368	Segmentation of rat spinal cord in PET using spatiotemporal information. , 2010, , .		0
369	Evaluation of a 3D point spread function (PSF) model derived from Monte Carlo simulation for a small animal PET scanner. Proceedings of SPIE, 2010, , .	0.8	0
370	PET evaluation of the TSPO ligands [F-18]FEPPA, [F-18]PRB06, and [F-18]PBR111 in nonhuman primate. NeuroImage, 2010, 52, S147.	2.1	0
371	Yale Center for Clinical Investigation: Leveraging Industry Partnerships and Research Cores. Clinical and Translational Science, 2012, 5, 435-436.	1.5	0
372	List-mode reconstruction for the FOCUS-220 with motion correction and spatially-variant probability density functions: Application to awake monkey imaging. , 2012, , .		0
373	Dynamic assessment of head motion compensation for the HRRT. , 2012, , .		0
374	Feasible uniform-resolution penalized likelihood reconstruction for static- and multi-frame 3D PET. , 2013, , .		0
375	P3-143: Amyloid burden is associated with decreased gray matter volume but not episodic memory performance in cognitively normal first-degree relatives at varying ApoE4 risk for Alzheimer's disease. , 2015, 11, P680-P681.		0
376	IC-P-101: Amyloid burden is associated with decreased gray matter volume but not episodic memory performance in cognitively normal first-degree relatives at varying ApoE4 risk for Alzheimer's disease. , 2015, 11, P69-P69.		0
377	18. In Vivo Quantification of mGluR5 Availability in Posttraumatic Stress Disorder. Biological Psychiatry, 2017, 81, S8.	0.7	0

378 Strategies to Improve Direct EM Patlak Reconstructions. , 2017, , .

#	Article	IF	CITATIONS
379	P2â€365: PET IMAGING OF SYNAPTIC DENSITY (SYNAPTIC VESICLE GLYCOPROTEIN 2A, SV2A) IN ALZHEIMER'S DISEASE: INITIAL EXPERIENCE. Alzheimer's and Dementia, 2018, 14, P832.	0.4	0
380	ICâ€04â€03: PET IMAGING OF METABOTROPIC GLUTAMATE RECEPTOR 5 BINDING IN ALZHEIMER'S DISEASE. Alzheimer's and Dementia, 2018, 14, P8.	0.4	0
381	ICâ€Pâ€183: PET IMAGING OF SYNAPTIC DENSITY (SYNAPTIC VESICLE GLYCOPROTEIN 2A, SV2A) IN ALZHEIMER'S DISEASE: INITIAL EXPERIENCE. Alzheimer's and Dementia, 2018, 14, P152.	0.4	0
382	F3. Imaging Alpha7 Nicotinic Acetylcholine Receptors in Individuals With PTSD. Biological Psychiatry, 2018, 83, S237-S238.	0.7	0
383	S13. IN VIVO EVIDENCE OF REDUCED SYNAPTIC VESICLE DENSITY IN SCHIZOPHRENIA USING [11C] UCB-J PET IMAGING. Schizophrenia Bulletin, 2019, 45, S310-S311.	2.3	0
384	P4â€481: ASSOCIATION BETWEEN ENTORHINAL CORTICAL TAU ACCUMULATION AND HIPPOCAMPAL SYNAPTIC DENSITY IN OLDER INDIVIDUALS WITH NORMAL COGNITION AND EARLY ALZHEIMER'S DISEASE: PRELIMINARY EXPERIENCE. Alzheimer's and Dementia, 2019, 15, P1497.	0.4	0
385	ICâ€Pâ€140: ASSOCIATION BETWEEN MGLUR5 AND SYNAPTIC DENSITY: A MULTIâ€TRACER STUDY IN HEALTHY A AND ALZHEIMER'S DISEASE. Alzheimer's and Dementia, 2019, 15, P115.	NGING 0.4	0
386	F33. In Vivo Brain Imaging of 11beta-Hydroxysteroid Dehydrogenase, a Marker of Cortisol Production, in PTSD. Biological Psychiatry, 2019, 85, S225.	0.7	0
387	PBR28 Brain PET imaging with lipopolysaccharide challenge for the study of microglia function in Alzheimer's disease. Alzheimer's and Dementia, 2020, 16, e037792.	0.4	0
388	The aging rhesus macaque as a potential model for Alzheimer's disease/dementia: An in vivo study of [ 11 C]PIB, [ 11 C]UCBâ€j, [ 18 F]MKâ€6240 and working memory performance. Alzheimer's and Dementia, 2020, 16, e038467.	0.4	0
389	11Câ€PBR28 brain PET imaging with lipopolysaccharide challenge for the study of microglia function in Alzheimer's disease. Alzheimer's and Dementia, 2020, 16, e043584.	0.4	0
390	Association between cerebral amyloid accumulation and synaptic density in Alzheimer's disease: A multitracer PET study. Alzheimer's and Dementia, 2020, 16, e043631.	0.4	0
391	Characteristics of Neurotransmitter Competition Studies Using Constant Infusion of Tracer 1 1Transcripts of the BRAINPET97 discussion of this chapter can be found in Section VIII , 1998, , 435-439.		0
392	Novel Use of Agent 11C-PHNO for Pet CT Imaging of Pancreatic Beta-Cell Mass. Diabetes, 2018, 67, .	0.3	0
393	Reply: 11C-(+)-PHNO Trapping Reversibility for Quantitative PET Imaging of Î <sup>2</sup> -Cell Mass in Patients with Type 1 Diabetes. Journal of Nuclear Medicine, 2020, 61, 1693-1693.	2.8	0
394	Translational PET Imaging of Spinal Cord Injury with the Serotonin Transporter Tracer [11C]AFM. Molecular Imaging and Biology, 2022, , 1.	1.3	0
395	Multimodal neuroimaging of metabotropic glutamate 5 receptors and functional connectivity in alcohol use disorder. Alcoholism: Clinical and Experimental Research, 2022, , .	1.4	0

Accelerating PET Image Reconstruction with CUDA. , 2022, , .